Interaction of Lipid Bilayer with Functionalized Gold Nanoparticles

M.Sc. Thesis

By
Ananya Patnaik
1603131004

DISCIPLINE OF CHEMISTRY
INDIAN INSTITUTE OF TECHNOLOGY INDORE
JUNE 2018

Interaction of Lipid Bilayer with Functionalized Gold Nanoparticles.

A THESIS

Submitted in partial fulfillment of the
requirements for the award of the degree
of
Master of Science

by

Ananya Patnaik

DISCIPLINE OF CHEMISTRY
INDIAN INSTITUTE OF TECHNOLOGY INDORE
JUNE 2018

INDIAN INSTITUTE OF TECHNOLOGY INDORE

CANDIDATE'S DECLARATION

I hereby certify that the work which is being presented in the thesis entitled **Interaction of Lipid Bilayer with Gold Nanoparticles** in the partial fulfillment of the requirements for the award of the degree of **MASTER OF SCIENCE** and submitted in the **DISCIPLINE OF CHEMISTRY, Indian Institute of Technology Indore**, is an authentic record of my own work carried out during the time period from July 2017 to June 2018 under the supervision of Dr. Anjan Chakraborty, Associate Professor, IIT Indore.

The matter presented in this thesis has not been submitted by me for the award of any other degree of this or any other institute.

Ananya Patnaik

This is to certify that the above statement made by the candidate is correct to the best of my/our knowledge.

Dr. Anjan Chakraborty

Ananya Patnaik has successfully given his M.Sc. Oral Examination held on **06 July 2018**.

Signature of Supervisor of MSc thesis
Date:

Convener, DPGC
Date:

Signature of Dr. S. S. Bulusu
Date:

Signature of Dr. M. N. Mahato
Date:

ACKNOWLEDGEMENT

I would like to thank my supervisor, **Dr. Anjan Chakraborty** for his guidance during this research work. I thank him not only for providing lab facility but also for motivation and constructive criticism.

I will also like to thank **Dr. Satya S. Bulusu** and **Dr. Manavendra N. Mahato** for their valuable suggestions in various aspects.

I am thankful to **Ms. Nishu Kanwa** who helped me in the entire course of this project. I am also grateful to **Mr. Soumya Kanti De** and **Mr. Mirajuddin Ahamed** for their help and cooperation.

Further I extend my gratitude to my classmates for their selfless support.

Finally I would like to thank Sophisticated Instrumentation Center (SIC), IIT Indore and IIT Indore for providing infrastructure and all others who inspired, helped and supported me in any way they could.

Ananya Patnaik

Abstract

We have investigated the interaction of functionalized anionic Gold nanoparticles (Au NPs) with DMPC (1,2-dimyristoyl-sn-glecerol-3-posphocholine), a phospholipid bilayer. In this study, Citrate-capped Au NPs, 3-mercaptopropanoic acid (MPA) functionalized Au NPs and Glutathione (GSH) functionalized Au NPs have been used. Membrane sensitive probes called PRODAN (6-propionyl-1,2-dimetylaminonaphthalene) and ANS (8-anilino-1-naphthalenesulphonate) were used to study the interaction between these Au NPs with the lipid bilayer through steady state and time resolved spectroscopy. We observed that the Au NPs bring stability to the bilayer. Also, the extent of interaction of Au NPs with the lipid bilayer was dependent upon the surface ligands used to functionalize those Au NPs. Citrate-capped Au NPs increased the phase transition temperature of the bilayer, upon interaction. We also explored the scope of interaction at different temperatures when the bilayer is present in the different phases; i.e. Liquid crystalline phase and Sol-gel phase. We performed confocal laser scanning microscopy (CLSM) imaging to demonstrate the surface modification in the bilayer due to interaction with Au NPs.

.

CONTENTS

LIST OF FIGURES

LIST OF TABLES

ACRONYMS

Au NP	Gold Nanoparticle
MPA	3-mercaptopropanoic acid
GSH	Glutathione
PRODAN	6-propionyl-1,2-dimethylaminenaphthalene
ANS	1-anilinonaphthalene-8-sulphonic acid
TCSPC	Time-Correlated Single-Photon Counting
TEM	Transition Electron Microscopy
DMPC	1,2-dimyristoyl-sn-glycero-3-phosphocholine
SUV	Small Unilamellar Vesicle
LUV	Large Unilamellar Vesicle
GUV	Giant Unilamellar Vesicle
DPPC	1,2-dipalmitoyl-sn-glycero-3-phosphocholine

NOMENCLATURE

nm	Nanometer
nM	Nano molar
°C	Degree Centigrade
g	Gram
τ_i	Lifetime of i^{th} component
χ^2	Reduced chi-square
a_i	Amplitude of the i^{th} component in a multiexponential decay
T_m	Phase Transition Temperature
ZnO	Zinc oxide
Cit	Citrate
$HAuCl_4$	Trichlorogold hydrochloride
keV	Kilo electron volt
µM	Micro molar
D(t)	Normalized Fluorescence Decay
Ar	Argon

1) INTRODUCTION

1.1) Lipid Bilayers (Liposomes): Cells are the building blocks of life and each cell has a cell membrane that separates the interior of the cell from the outside environment [1]. A cell membrane is composed of phospholipids and membrane proteins [2] having lipid bilayer as its universal component. A lipid bilayer has a very critical role because its structural components provide the barrier that encloses the boundaries of a cell [3].

Lipid bilayers, or liposomes, are composed of two layers of fat cells organized in two sheets. Lipids are fats that are insoluble in water. There are two important parts of a lipid that fabricate a lipid bilayer. First is a hydrophilic part, also called a polar head group, and second, a hydrophobic part, or nonpolar tail containing long hydrocarbon chain. Basically, lipid molecules organize themselves spontaneously to form a bilayer (in polar medium like water), to hide their hydrophobic parts and expose the hydrophilic regions to solvent molecules [3].

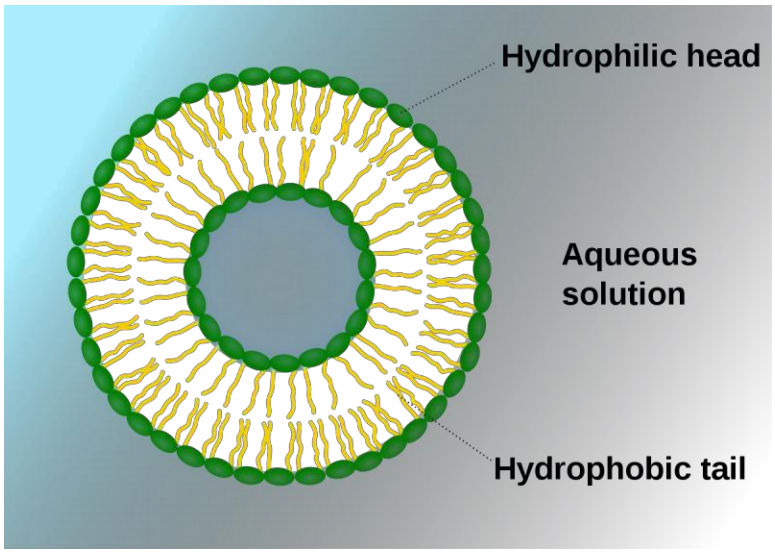

Figure 1: Structure of liposome showing hydrophilic head and 11hydrophobic tail. [1]

As discussed earlier, the cell membrane is composed of mainly phospholipids and membrane proteins. The phospholipids construct the lipid bilayer by binding at the hydrophobic group of each other to form a sphere. Therefore, the liposome formed from the phospholipids is generally utilized as the cell membrane model [2]. The liposomes prepared from such lipids are called the PC liposomes.

Lipid bilayer membranes have been a subject of great interest in the recent past, owing to their sensitivity in terms of phase transition temperature, hydration and dehydration upon interaction with several nanoparticles, polymers and metal ions etc. [4-11]. There are a lot of methods used synthesize lipid bilayers from lipid molecules such as detergent dialysis [12], reverse-phase evaporation [13], thin film hydration [14], and solvent injection [15]. The lipid bilayers can be categorized into various groups on the basis of their size: SUV- Small Unilamellar Vesicle (20-100 nm), LUV- Large Unilamellar Vesicle (> 100 nm), GUV- Giant Unilamellar Vesicle (>1μm) and MLV- Multi-Lamellar Vesicle (>0.5μm). Commercially there are a number of lipids available which can be used to synthesize PC liposomes in the lab. Some of them are 1,2-dipalmitoyl-sn-glycero-3-phosphocholine (DPPC, T_m 41°C for 16:0 PC), 1,2-dimyristoyl-sn-glycero-3-phosphocholine (DMPC, T_m 24°C for 14:0 PC) etc.

An important property of a lipid bilayer is the relative fluidity (mobility) of each of the lipid molecules and how this fluidity is affected by temperature [1]. Basically, at a given temperature, a lipid can exist in one of the two phases, namely: sol-gel phase and liquid crystalline phase. At phase transition temperature for any lipid, there is a particular temperature at which a change in its physical state is induced [1]. At this temperature a lipid molecule undergoes transition from the ordered gel phase, where the hydrocarbon chains are fully extended and closely packed, to the disordered liquid crystalline phase where the hydrocarbon chains are randomly oriented and fluid [16]. This is known as the phase transition temperature of

the lipid. The actual phase in which a lipid can exist at a particular temperature is decided by its phase transition temperature. The PC liposomes usually show aggregation when the temperature is decreased below the gel-to-liquid-crystalline phase transition temperature of vesicle membrane and by addition of certain polymers [17-20].

The lipid bilayers gain stability upon alterations in pH, ionic strength, and addition of polyvalent ions [21]. The changes in the phase transition temperature of the bilayer, induced due to such interactions, greatly affect the membrane polarity, fluidity, order and surrounding water content [4-11, 22-25]. For example, the introduction of guest molecules, such as cholesterol and proteins strongly modifies the membrane properties and brings in stability and order [10-11, 22-25]. Furthermore, interactions between lipid bilayers and metal nanoparticles are also an emerging area of research these days as they usually result into distinctly biocompatible systems [26-31] These systems have immense applications in various fields like imaging, drug delivery, separation and bio sensing [29-33].

Liposomes are acceptable drug carriers and that can be used for transportation hydrophilic and lipophilic drugs as well as their protection from degradation [34]. Mostly, for all of the drugs their therapeutic and toxic concentrations are alarmingly close to one another [35]. So, there is a high chance that these drugs can cause cytotoxicity. As a solution, liposomal formulations have been fabricated to achieve enhanced therapeutic activity with reduced toxicity [36].

1.2) Nanoparticles: As mentioned earlier, the interaction between lipid bilayers and metal nanoparticles is emerging as an interesting field to explore due to the resultant biocompatible systems [26-31]. There are several reports involving the adsorption of nanoparticles by zwitterionic lipid bilayers, some of them are known to bring in stability to the membrane [30, 37-39]. As a result, considerable progress has been achieved on fabrication of different kinds of nanoparticles (NPs) which has led to the discovery of their

very interesting properties. Metal nanoparticles have potential applications in catalysis, sensing, magnetics, optics, and electronics [40]. Some of the NPs like gold [41] or quantum dots [42] have proven to be potential candidates for diagnostics and therapeutics [43-45]. ZnO nanoparticles have been applied in broad fields, including electronic materials, rubber manufacture, biosensors, sunscreens pigments, and food additives [46]. Mn_5Si_3 nanoparticles have been synthesized to achieve ferromagnetic ordering [47].

There are several reports showcasing evidence for the adsorption of nanoparticles by zwitterionic lipid bilayers. In fact some of them even bring stability to the membrane [30, 37-39]. Out of all such materials, gold nanoparticles are of great significance. The surface chemistry of gold nanoparticles can be easily controlled by various capping agents, mainly with thiol ligands [48-51]. They are also known to exhibit a strong van der Waals interaction giving rise to a strong physisorption and low colloidal stability [52].

Gold nanoparticles show distance-dependent color due to surface Plasmon coupling, which makes them easy to monitor visually [53-54]. It has been reported that lipid bilayers remain more intact and lose their tendency to fuse with one another when coated with adsorbed nanoparticles with a high charge density on the surface of the bilayer, even when the surface is covered by 25% [39]. Hence, the perfect combination of NPs with liposomes is desirable for various applications. Here we have studied the interaction of DMPC bilayer with differently capped/ functionalized gold nanoparticles.

1.3) Fluorescent Molecular Probes: Although innumerous studies have been done on the interactions of lipid bilayers and gold nanoparticles, the literature lacks sufficient studies that involve the spectroscopic studies of these interactions. In this context, fluorescent molecular probes are of

immense significance to monitor the changes in the fluorescent parameters of the lipid bilayer membrane. Several fluorescent probes which are particularly sensitive to membrane polarity, can reveal changes in terms of emission wavelength and intensity as well as lifetime decay and anisotropy [55-64]. Amongst the spectral sensitive probes, PRODAN (6-Propionyl-2-Dimethylaminonaphthalene) and ANS (8-anilino-1-naphthalenesulphonate) are particularly interesting because both these fluorescent probes are sensitive to the dielectric constant and polarity of the surrounding media. The Photophysical behavior of PRODAN and ANS in aqueous and membrane media have been well studied in literature [55-64]. A significant red shift of the PRODAN emission is observed with increasing solvent polarity, owing to dipolar relaxation phenomenon [56-57]. However, in case of ANS, the Charge Transfer (CT) state in a polar medium decays to the ground state via electron transfer process resulting in quenched fluorescence. The intense blue fluorescence in hydrophobic environment is mostly due to the restricted rotational motion of the phenylamino group of ANS [55].

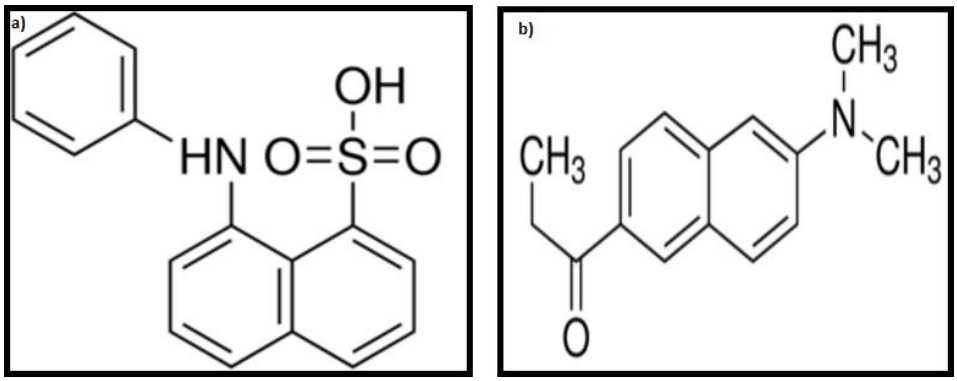

Figure 2: Molecular structure of a) ANS* and b) PRODAN**

1.4) Motivation of Proposed Work Plan: It has been earlier reported that functionalized gold nanoparticles interact with liposomes and bring about the latter's stability [3]. In view of the above discussion, the membrane sensitivity of the probes, PRODAN and ANS, towards changes in the surface properties of the phosphocholine zwitterionic lipid 1,2-dimyristoyl-sn-glycero-3-phosphocholine (DMPC) membrane was explored, upon interaction with differently functionalized anionic gold nanoparticles (AuNPs). Here, the interactions of DMPC bilayer with Citrate-capped AuNPs (Cit-AuNPs), AuNPs functionalized with mercaptopropionic acid (MPA-AuNPs) and with glutathione (GSH-AuNPs) was studied at different temperatures. Basically, we have endeavored to investigate the effect of the bulkiness of the surface ligands, which are used to functionalize the nanoparticles, on their interaction with lipid bilayers.

2)EXPERIMENTAL SECTION

2.1) Materials: Phospholipid (DMPC), $HAuCl_4$, PRODAN, ANS, 3-mercaptopropionic acid and trisodium citrate were bought from Sigma-Aldrich. Glutathione was purchased from SRL. Phosphate buffer salts were purchased from Merck. All materials were used as received. In all cases, Milli-Q water was used to prepare the solutions.

2.2) Lipid bilayer Preparation: DMPC Lipid bilayer was prepared in phosphate buffer saline (PBS, pH = 7.4, I = 0.01 M). DMPC was dissolved in ethanol (0.01% of the hydrating solution) and injected in a preheated PRODAN or ANS solution above the phase transition of DMPC (at ~45 °C). The solution was stirred at this temperature for nearly an hour, and cooled down to room temperature before performing any further studies. The total concentration of the lipid (DMPC) was fixed at 0.6 mM, while that of PRODAN and ANS was fixed at 2 µM and 4 µM, respectively for all of the experiments.

2.3) Synthesis of Citrate-capped Gold nanoparticles: Citrate-capped Au NPs were synthesized following the classical citrate reduction of $HAuCl_4$, using a previously described protocol with slight modification [49]. All glasswares used for the synthesis were cleaned in freshly prepared aqua regia solution, rinsed with Milli-Q water and dried in oven. Briefly, trisodium citrate solution (38.8 mM, 10 mL) was rapidly injected to a boiling $HAuCI_4$ solution (1.0 mM, 100 mL) under vigorous stirring. The resulting wine-red colored colloidal solution was boiled for 30 minutes, cooled down to room temperature and stored at 4 °C for further use.

2.4) Functionalization of gold nanoparticles: Citrate capped Au NPs were functionalized with MPA and GSH, following a previously described protocol with slight modification [65]. Briefly, MPA (25 mM, 10 µL) or GSH (25 mM, 10 µL) was added to Citrate-capped Au NPs (13.4 nM, 746 µL) and incubated overnight, and stored at 4 °C for further use.

2.5) Instrumentation: Tecnai T20 transmission electron microscope with an operating voltage of 200 keV was used for conducting HR-TEM study to reveal the morphology of the synthesized Citrate-capped An NPs. Absorption spectra of the Au NPs were recorded using a Varian UV-Vis spectrophotometer (Carry 100 Bio) in a quartz cuvette (10 × 10 mm).

Fluoromax-4p spectrofluorometer from Horiba JobinYvon (model: FM-100) was used for recording steady-state fluorescence spectra. The liposome−nanoparticle interaction was studied by changing the concentration of gold nanoparticles in a fixed concentration of lipid and PRODAN or ANS. In brief, we prepared a set of solutions in different volumetric flasks that contained 2 μM PRODAN, 0.6 mM lipid, 4 μM ANS and different concentrations of Au NPs. The samples were excited at 375 nm. The fluorescence spectra were corrected for the spectral sensitivity of the instrument. The excitation and emission slits were 2 nm each for all of the PRODAN and ANS emission measurements. In all of the titration experiments, we maintained pH = 7.4, I = 0.01 M, and the desired experimental temperature.

A picosecond TCSPC machine from Horiba (Fluorocube- 01-NL) was used for time-correlated single-photon counting (TCSPC). The samples were excited at 375 nm using a picosecond diode laser (model: Pico Brite-375L), and the decays were collected at 440 and 500 nm. A filter was used on the emission side to eliminate the scattered light. The signals were collected at magic angle (54.75°) polarization using a photomultiplier tube (TBX-07C) as the detector. The full width at half-maximum (FWHM) of the instrument response function of the setup was ∼140 ps. The data analysis was performed using IBH DAS version 6 decay analysis software. Throughout all of the titration experiments, we maintained pH = 7.4, I = 0.01 M, and the desired experimental temperature.

The decays were fitted with a multiexponential function:

$$D(t) = \sum_{i=1}^{n} a_i \exp\left(\frac{-t}{\tau_i}\right) \quad (1)$$

Here D(t) denotes normalized fluorescence decay and a_i is the normalized amplitude of decay components τ_i, respectively. The average lifetime was obtained from the equation:

$$\langle \tau \rangle = \sum_{i=1}^{n} a_i \tau_i \quad (2)$$

The quality of the fit was judged by reduced chi square (χ^2) values and corresponding residual distribution. The acceptable fit has a χ^2 near unity.

A confocal microscope from OLYMPUS, model no. IX-83 was used for confocal imaging of the samples. A Multiline Ar laser (gas laser) with an excitation wavelength of 488 nm was used. The observation mode was LSM (laser scanning microscopy), the scan mode was XY, and the scan direction was one way. The liquid samples were dropped on glass slides and fixed with coverslips before imaging.

3) RESULTS AND DISCUSSION

3.1) Characterization of functionalized Gold nanoparticles: Three types of differently functionalized anionic gold nanoparticles were first synthesized and characterized, including 1) Citrate capped Au NP, 2) MPA functionalized Au NP and 3) GSH functionalized Au NP. **Figure 3 a** shows the chemical structures of the different surface ligands used to functionalize the Au NPs. The citrate group bound to Au NPs can be easily replaced by thiol-bearing ligands [48, 50, 65-66] .UV-Vis absorption spectra reveal that the nanoparticle monodispersity is maintained after the ligand exchange as illustrated in **Figure 3 b**.

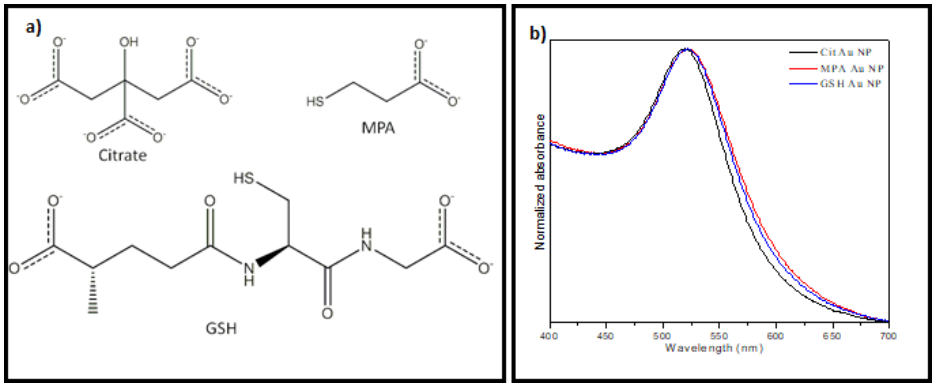

Figure 3: a) Structure of Citrate, MPA and GSH and b) UV-Vis spectra of Citrate capped, MPA- and GSH functionalized Au NPs

These nanoparticles are obtained by the simple ligand exchange of citrate capped Au NPs with MPA and GSH respectively, and thus possess an identical core diameter. Pure Citrate-stabilized gold nanoparticles display a surface Plasmon resonance (SPR) band at 521 nm, which is a characteristic of isolated spherical gold nanoparticles[50-51, 66-67].

A similar Plasmon band is obtained for MPA-Au NP and GSH-Au NP, and there appeared no shift in the SPR wavelength. This indicates that the Au NPs remained unaggregated and were highly stable.

Au NPs were characterized by TEM, which indicates a narrow distribution of the diameter (12-14 nm), as shown in **Figure 4 (a, b)**.

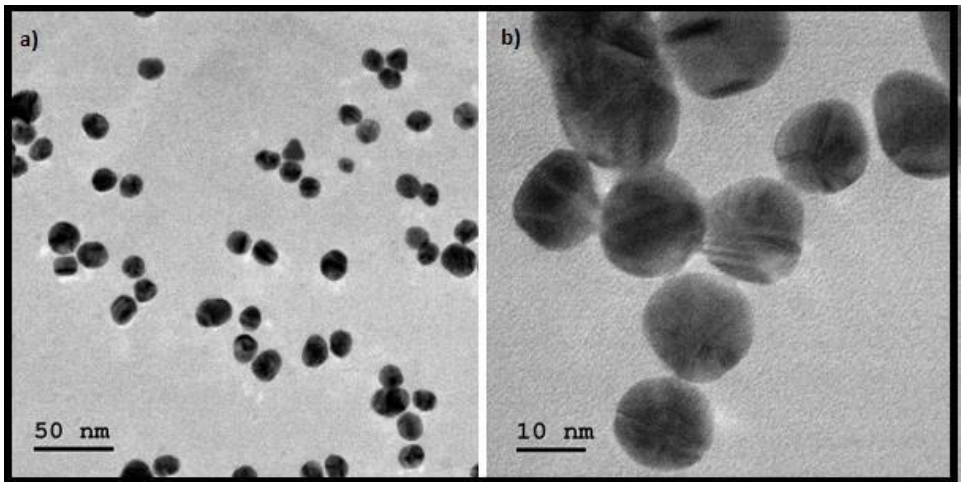

Figure 4: Representative TEM images of Citrate Au NPs

Zeta potential measurements reveal that all the synthesized nanoparticles are negatively charged, clearly seen in **Figure 5.**

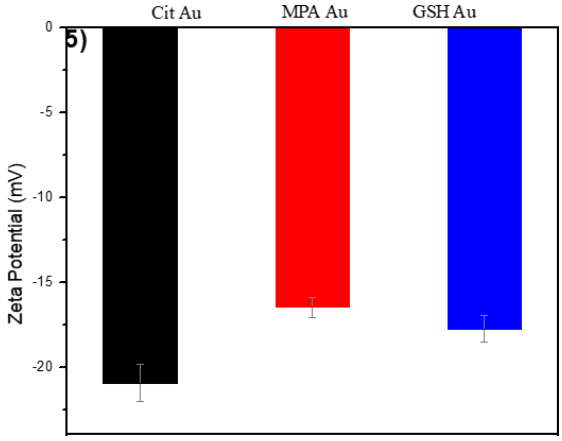

Figure 5: Zeta potential measurements of Citrate-capped, MPA- and GSH functionalized Au NPs

Citrate-capped Au NPs bearing a surface charge of -20.94 ± 1.1 mV; while MPA and GSH functionalized Au NPs have a charge of -16.47 ± 0.6 mV and -17.73 ± 0.8 mV, respectively. This change in Zeta potential measurements indicates the functionalization of Au NPs with the negatively charged ligands.

The concentration of the capping agents was kept so that no aggregation of the nanoparticles takes place. All these nanoparticles obtained were water-soluble and stable in aqueous solutions, with no aggregation observed for a period of one month when stored at 4 °C.

3.2) Interaction of gold nanoparticles and lipid bilayer using PRODAN:

Being a membrane sensitive probe, PRODAN shows an emission at 527 nm in aqueous medium. This emission band is assigned to Charge transfer (CT) state. But in the presence of less polar medium like lipid bilayer, another emission band arises at around 435-440 nm, which is due to its locally excited (LE) state. The emission spectra for PRODAN, with and without the presence of a non-polar medium is illustrated in **Figure 6.** The LE band indicates that PRODAN is partitioned in lipid bilayer [3]. This interesting feature of PRODAN makes the spectral studies easier to analyze. Here, DMPC was used, which has a phase transition temperature of 24 °C, for studying the interaction with differently functionalized gold nanoparticles.

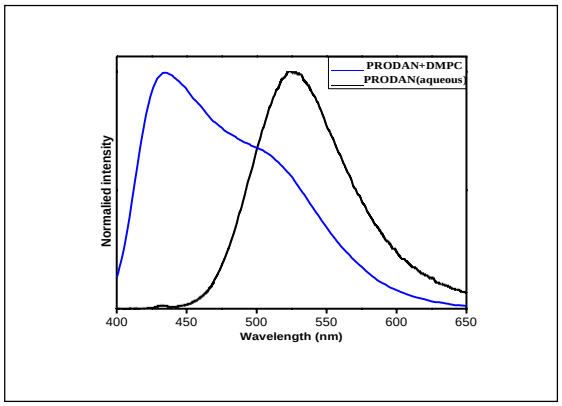

Figure 6: Emission spectra of PRODAN with and without the presence of lipid (DMPC).

It can be seen that the emission spectra of PRODAN is shifted to a shorter wavelength upon interaction of the lipid bilayer with all three anionic nanoparticles (**in figure 7**) , while a maximum blue shift was observed for Citrate-capped Au NPs, followed by MPA-functionalized Au NPs and least in GSH-functionalized Au NPs. This observation is more clearly evident from the area fraction plot, which reveals that the band corresponding to LE state increases inordinately for Citrate-capped Au NPs.

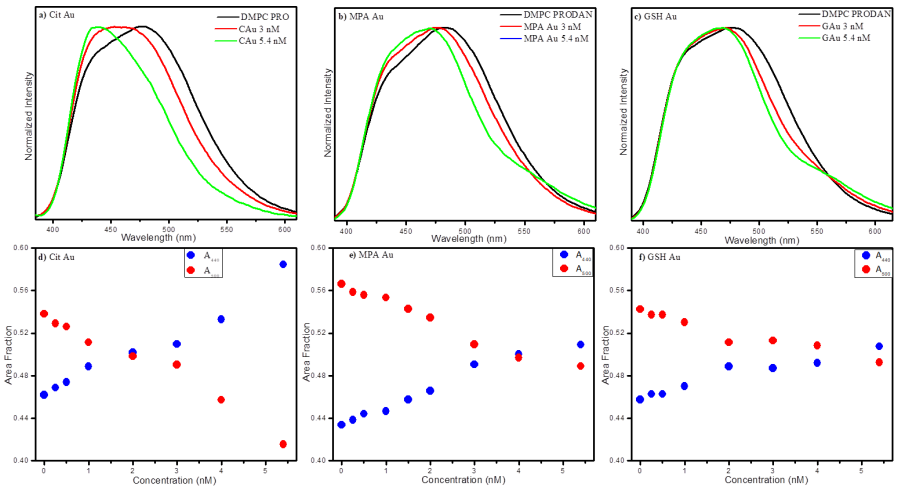

Figure 7: Normalized emission spectra for the addition of Au NPs in different concentrations (0 to 5.4 nM) in DMPC−PRODAN solution for (a) Citrate Au NPs, (b) MPA Au NPs, and (c) GSH Au NPs and their corresponding area fraction versus concentration of Au NPs plots (d-f) for DMPC liposomes at 440 (blue emission) and 500 nm (red emission) at 25 °C.

It was observed that the blue shift was maximum in the case of Citrate-capped Au NPs followed by MPA-functionalized Au NPs. GSH-capped Au NPs caused the least blue shift out of the three. This observation can be

more elaborately explained by the area fraction plot in **Figure 7 (d-f)** which shows that the band corresponding to the L.E. state of PRODAN is more pronounced in case of lipid bilayers interacting with the Citrate-capped Au NPs than that with MPA- and GSH functionalized Au NPs. This indicates that the lipid bilayer upon interaction with Citrate–capped Au NPs is the least hydrated at room temperature of 25°C. It is also quite obvious that the adsorption efficiency of the different Au NPs varies significantly. The Citrate-capped Au NPs exert a relatively stronger Van der Waal's force which affects the bilayer packing as is brings it to a stronger gel phase. MPA-capped Au NPs can still be efficiently absorbed, owing to the small size of the ligand (~0.3 nm). Since MPA is relatively shorter thiolated carboxyl molecule, the capping of Au NPs with MPA results into stronger adsorption on the surface of the lipid bilayer as compared to the more bulky GSH group, which rather reduces the adsorption efficiency. . These surface ligands separate the Au NP core from the bilayer surface, which results into a decrease in the van der Waals force between the bilayer surface and the Au NP core. The Van der Waals interaction are short ranged hence, even a small separation by the surface ligand from the Au NP core is sufficient to cause changes in the adsorption strength [38]. Interestingly, the bulkiness of the surface ligands, not their structure, plays an important role in interaction of the Au NPs with the lipid bilayers [48].

To further establish these results, lifetime and anisotropy decay measurements of PRODAN in presence of DMPC were conducted, upon addition of various Au NPs. Intensity decays were collected at 440 nm and 500 nm wavelengths. In the following figure **(Figure 8)**, the decay collected at 500nm is shown.

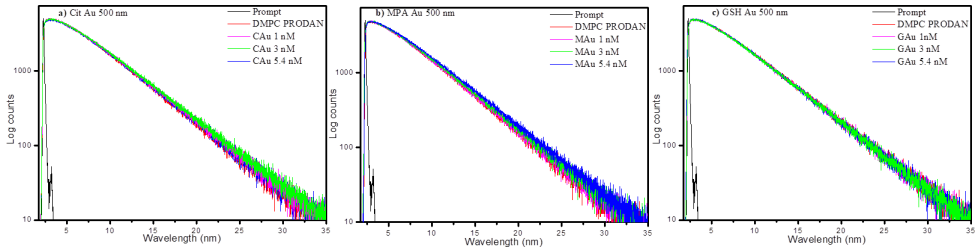

Figure 8: Lifetime decay of PRODAN for DMPC at different concentrations of Au NPs for a) Citrate-Au NPs, b) MPA-Au NPs, and c) GSH-Au NPs at 500 nm at 25 °C.

It is observed that in DMPC liposomes, the decays at 500 nm remain intact upon addition of all the three different Au NPs. The intensity decays collected at 440 nm at 25°C are shown in the following **Figure 9.**

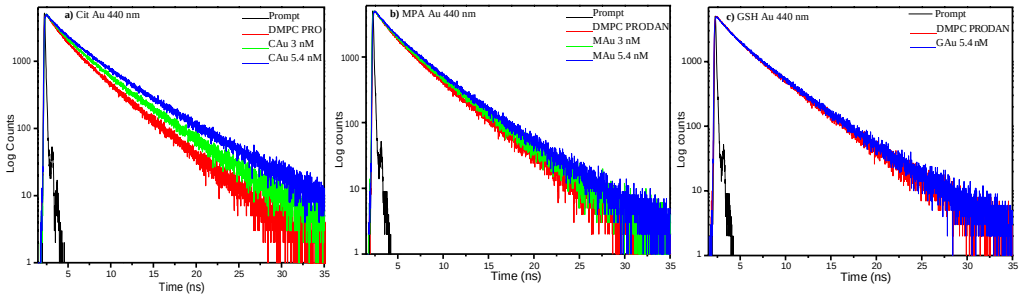

Figure 9: Time-resolved decay curves of PRODAN in DMPC−Au NPs solutions at different concentrations of Au NPs for Citrate-Au NPs (a), MPA-Au NPs (b) and GSH-Au NPs (c) at 25°C.

TABLE 1: @440 nm						
Sample	**τ_1 (ns)**	**τ_2 (ns)**	**a_1**	**a_2**	**χ^2**	**<T>(ns)**
DMPC	1.09	3.83	0.43	0.57	1.05	2.66
DMPC + Citrate-Au NPs	1.55	5.15	0.42	0.58	1.10	3.63
DMPC + MPA-AuNPs	1.30	4.10	0.41	0.59	1.08	2.94
DMPC + GSH-AuNPs	1.20	3.71	0.40	0.60	1.10	2.71

Experimental error is within 5-10%

Table 1: Lifetime Components, Normalized Amplitudes of Lifetime Components, and Average Lifetime of PRODAN at Different Concentrations of Au NPs at 440 nm at 25 °C.

Moreover, anisotropy measurements revealed that the rotational relaxation of DMPC bilayer increases up to a great extent upon adsorption of Citrate-capped Au NPs.

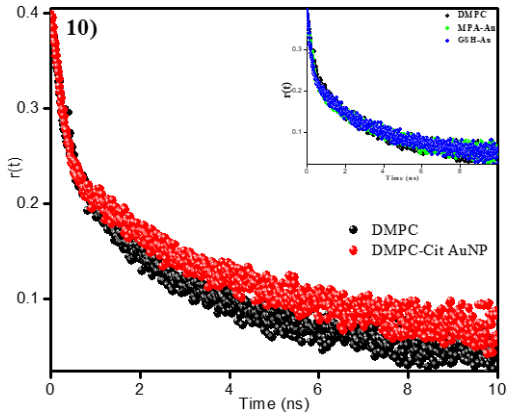

Figure 10: Anisotropy decays of PRODAN in a) DMPC, Cit-AuNP adsorption and DMPC, MPA- and GSH-AuNP adsorption (as shown in the inset) to the bilayer at 440 nm at 25 °C.

However, there wasn't any significant change observed in anisotropy in case of MPA- and GSH functionalized Au NPs to DMPC bilayer (**as shown in the inset**) This observation confirms that bare Au NPs bring about stability to the bilayer as they don't face any steric hindrance from bulky groups upon interaction, unlike MPA-and GSH functionalized Au NPs. Citrate-capped Au NPs replace the water molecules on the surface of the DMPC bilayer to bring about dehydration which causes its shrinkage.

It has been recorded earlier [3] that maximum gelation in a lipid bilayer occurs near its phase transition temperature. Hence, temperature dependent studies are of paramount importance as they help in observing the changes in phase transition of a lipid bilayer upon addition of various Au NPs. The sensitivity of PRODAN was exploited towards the temperature-induced phase transition for DMPC bilayer using temperature dependent emission intensity.

From **Figure 11 (a and b)**, it is clearly revealed that the fluorescence intensity of PRODAN corresponding to the LE state (435 nm) decreases and that of the TICT state (490 nm) increases with a rise in temperature, indicating that the bilayer membranes change their phase from a highly ordered and compact SG phase to fluidic LC (liquid crystalline) phase.

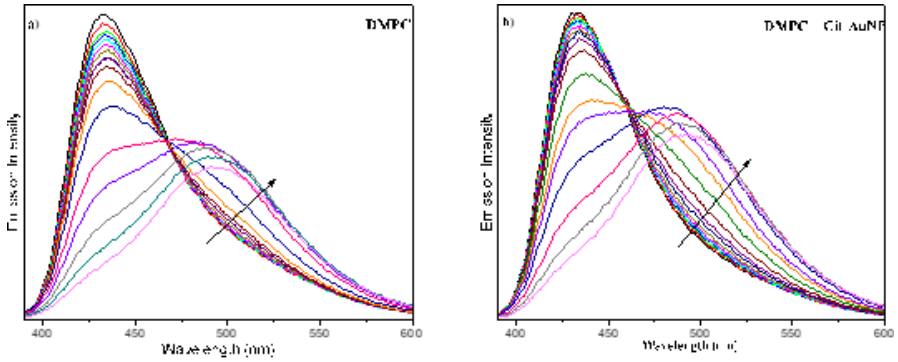

Figure 11: Plots of temperature-induced variation in the steady-state fluorescence spectra of PRODAN in DMPC vesicles; Fluorescence Emission intensity with change in temperature a) without Au NP addition and b) upon adsorption of Citrate-AuNPs to DMPC (Arrow indicates increase in temperature from 10 °C to 45 °C)

The spectral shift in the emission band of PRODAN can be explained on the basis of contribution of probe partitioning into the membrane and aqueous medium along with solvent relaxation phenomenon. PRODAN's partitioning into liquid crystalline phase is stronger as compared to that into sol gel phase. Hence, the peak representing the free aqueous PRODAN (i.e. 520) disappears as temperatures go higher than the phase transition temperature of the DMPC bilayer. A maximum limiting band is observed at around 490-500 nm [66]. The spectral shift is dependent only on the phase of the bilayer membrane. Here, its polar head group or its charge doesn't play any role.

To further analyze the alterations in the emission spectra of PRODAN, by plotting an area fraction curve (i.e. A_{435nm}/ $A_{490nm)}$ versus temperature. The decrease in fluorescence area at blue end is sigmoidal with a maximum change at the phase transition temperature of the bilayer as shown in the following **Figure 12 a**. This is more clearly notable in the derivative plot of fluorescence emission intensity (dA/dT) with varying temperature, as shown in the following **Figure 12 b**.

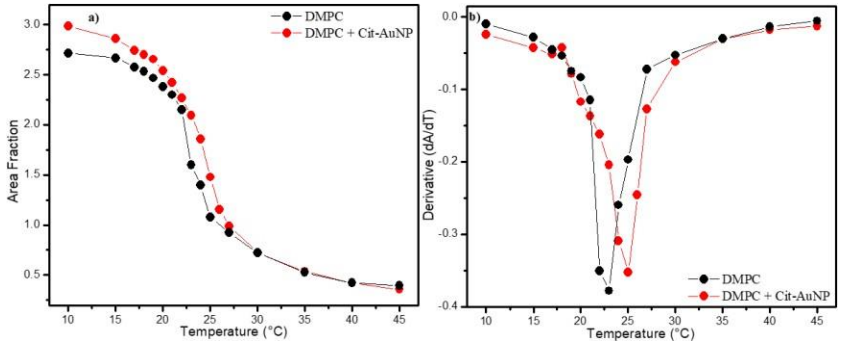

Figure 12: a) Area fraction ($A_{435\ nm}/A_{490\ nm}$) versus Temperature plot for DMPC-PRODAN in the presence and absence of Citrate-AuNPs b): First derivative of Area (dA/dT) versus Temperature plot. Here, [DMPC] = 0.6 mM, [PRODAN] = 2 μM and [Au NP] = 5.4 nM.

It is revealed that the phase transition temperature of the DMPC bilayer is observed at 23 °C, however, the addition of Citrate-AuNPs to the lipid bilayer results into further stabilization of the bilayer, which results in an increase in the phase transition from 23 °C to 25 °C. The addition of MPA and GSH-AuNPs did not show any effective changes on the phase transition temperature of DMPC bilayer. The electrostatic forces between the nanoparticles and the bilayer head group tightens the loosely packed lipid molecules around the Au-NP binding site. The adsorption of negatively charged Au-NPs is known to make the phosphatidylcholine (PC) lipid bilayer stiff, restructuring the bound lipid molecules into a raft phase [68-69]. This results in stitching of the bilayer, increasing its phase transition temperature.

Since DMPC is present in nearly Liquid Crystalline (LC) phase at 25 °C, changes corresponding to phase transition are more pronounced at this temperature. However, below this temperature when the bilayer is present in a more rigid Sol-Gel phase, we presume that only trivial changes might be observed. We performed the experiment at 15 °C to know the fate of the nanoparticles interaction with the lipid bilayer.

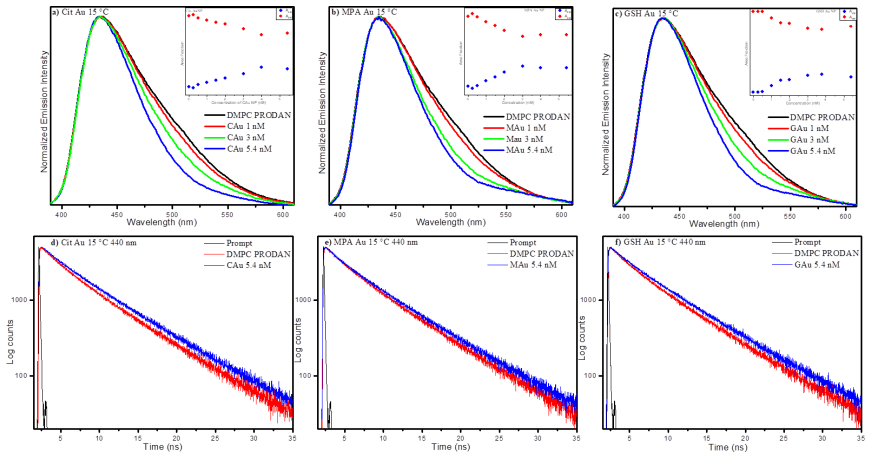

Figure 13: Normalized emission spectra for the addition of Au NPs in different concentrations (0 to 5.4 nM) to DMPC−PRODAN solution for (a) Citrate Au NPs, (b) MPA Au NPs, and (c) GSH Au NPs (inset shows area fraction v/s concentration plot); and corresponding Time-resolved decay curves of PRODAN in DMPC−Au NPs solutions at 440 nm (d-f) at 15 °C.

TABLE 2: @440 nm						
Sample	**τ_1 (ns)**	**τ_2 (ns)**	**a_1**	**a_2**	**χ^2**	**<T>(ns)**
DMPC	2.16	6.47	0.30	0.70	1.01	5.17
DMPC + Cit-Au NPs	2.48	6.92	0.24	0.76	1.04	5.85
DMPC + MPA-AuNPs	2.22	6.70	0.29	0.71	1.06	5.38
DMPC + GSH-AuNPs	2.30	6.88	0.24	0.76	0.99	5.78

Table 2: Lifetime Components, Normalized Amplitudes of Lifetime Components, and Average Lifetime of PRODAN at Different Concentrations of Au NPs at 440 nm at 15 °C.

From **Figure 13,** we observe that the peak corresponding to approximately 490 nm (CT state) in the emission spectra decreases upon the addition of all the three anionic Au NPs, which is also evident from the polarization plot (as shown in the inset). The lifetime decay at 440 nm also increases moderately for all the three Au NPs (data shown in **Table 2**)

Hence, at lower temperatures, the differently functionalized Au NPs are adsorbed on the bilayer surface to a more or less similar extent. Since DMPC is already at 15°C , it is very rigid a this temperature. As a result there is moderate effect in terms of instanteneous adsorption and gelation for all the nanoparticles. Interestingly, the maximum adsorption on the surface of DMPC bilayer occurs at 25°C as compared to temperatures above and below the phase transition temperature. We explain this observation by the fact that near the phase transition temperature of the lipid (T = 25 °C), DMPC remains in a nearly LC phase; thus, even a little increase in the phase transition temperature drastically alters DMPC from a nearly LC phase to a more compact SG phase.

It is reported that the lipid bilayer can be easily punctured (becomes softer) at temperatures close to the phase transition of the lipid. Thus the bilayer exhibits an anomalous softening and the ordering of the headgroup and that of the inter-bilayer water is the lowest at temperatures near the phase transition [70]. Thus any changes at the bilayer surface near the phase transition temperature that tend to stiffen the bilayer are very much pronounced and bring it to the more rigid SG phase. It has also been reported that an ion entering the hydrophilic headgroup region of the bilayer perturbs the membrane by pulling the headgroup inwards. The resulting defect lowers the overall energy barrier for the ion to pass. Temperatures above the phase transition facilitate this process [71]. However, the lipid bilayer is

least hydrated at temperatures below the phase transition of the lipid than in the fluid phase and chains condense to form a gel state [72]. Thus the effects are not much prominent when the bilayer is present in the SG phase, because the bilayer is tightly packed and the adsorption of the nanoparticles does not change the phase state of the bilayer.

Further, since the bilayer could not change the phase state upon interaction with AuNPs at 15 °C, we performed the experiment far above the phase transition of the lipid, i.e. at 35 °C when the bilayer is present in the liquid-crystalline (LC) phase. At a temperature above the phase transition temperature (i.e. 35 °C), we observe that a small blue shift takes place upon addition of AuNPs on the bilayer surface, indicating gelation, and the intensity corresponding to LE state increases as shown in the inset (**Figure 14)**.

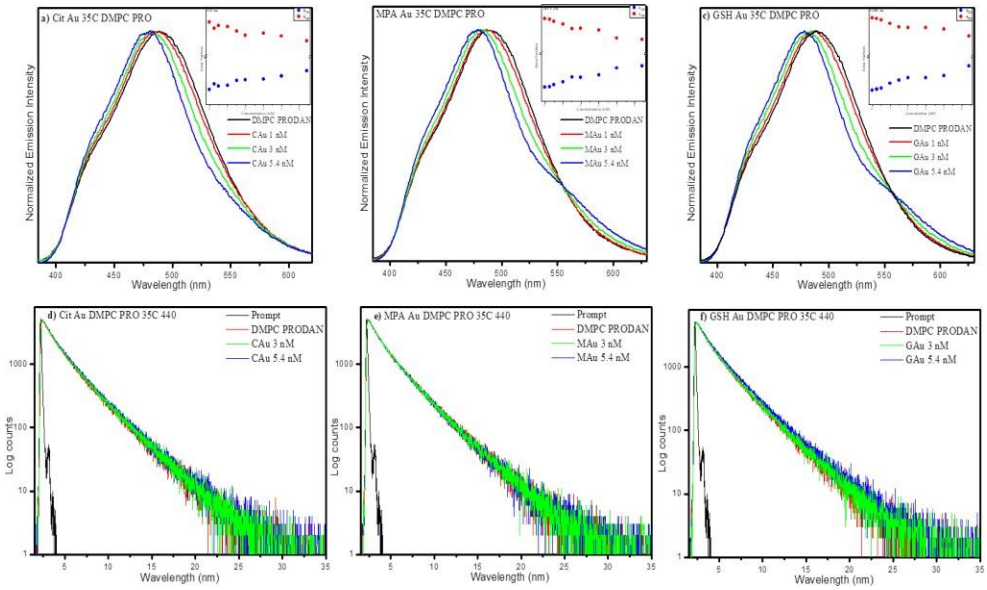

Figure 14: Normalized emission spectra for the addition of Au NPs in different concentrations (0 to 5.4 nM) to DMPC−PRODAN solution for (a) Citrate Au NPs, (b) MPA Au NPs, and (c) GSH Au NPs (inset shows area fraction plots); and

corresponding Time-resolved decay curves of PRODAN in DMPC−Au NPs solutions at 440 nm (d-f) at 35 °C.

TABLE 3: @440 nm						
Sample	**τ_1 (ns)**	**τ_2 (ns)**	**a_1**	**a_2**	**χ^2**	**<T>(ns)**
DMPC	0.98	2.99	0.50	0.50	1.16	1.98
DMPC + Cit-AuNPs	0.98	3.01	0.47	0.53	1.13	2.05
DMPC + MPA-AuNPs	0.96	3.00	0.50	0.50	1.24	1.98
DMPC + GSH-AuNPs	1.00	3.08	0.44	0.56	1.06	2.16

Experimental error is within 5-10%

Table 3: Lifetime Components, Normalized Amplitudes of Lifetime Components, and Average Lifetime of PRODAN at Different Concentrations of Au NPs at 440 nm at 35 °C.

However, there is apparently no change in the lifetime decay. This can be explained in the light of the fact that since DMPC remains in completely LC phase at 35 °C, it is not capable of holding more nanoparticles as compared to DMPC in SG or nearly LC phase. The higher increment in lifetime decay at lower temperature stems from the fact that DMPC being in SG phase or nearly LC phase occupies less area per lipid molecule, allowing it to capture more number of nanoparticles. Since the experimental temperature is far above the phase transition temperature of DMPC, it remains in LC state and any change, howsoever small, that occurs upon the addition of Au NPs cannot change the phase state of the lipid bilayer. It is

therefore, not possible to detect the small change that appears in the steady state, by lifetime measurements at 440 nm.

Another important observation from the steady state emission spectra (**Figure 14)** is that there emerges an emission band at around 540 nm upon addition of MPA and GSH-AuNPs. This band corresponds to the partitioning of PRODAN in aqueous medium. Given that the adsorption of Cit-AuNPs is strongest amongst the three anionic AuNPs, it tends to stabilize the bilayer to a higher extent by tightly binding to the surface of the bilayer. Therefore, the band corresponding to PRODAN in aqueous medium does not appear for Cit-AuNPs. However, it has already been discussed that MPA and GSH-AuNPs do not change the phase transition temperature of the lipid bilayer and the adsorption is comparatively weaker, there occurs a leakage of the probe in the aqueous medium. This free PRODAN that partitions into aqueous medium is responsible for the emerging band at ~540 nm.

Summarizing the above stated results, the lipid bilayer is brought to gelation and stabilized to a different extent at different temperatures. There is a scope for gelation, howsoever small, at all the experimental temperatures but the maximum extent of gelation is brought at a temperature just above the phase transition of the lipid. **Figure 15** represents the extent to gelation brought to the bilayer by the addition of Cit-Au NPs when the bilayer is present in different phases, i.e. SG (15 °C), LC (35 °C) and just above the phase transition of the temperature in nearly LC state (25 °C). A maximum blue shift is revealed, corresponding to a higher population of the LE state of PRODAN in the SG phase, followed by huge increment in the lifetime at this temperature and vice versa.

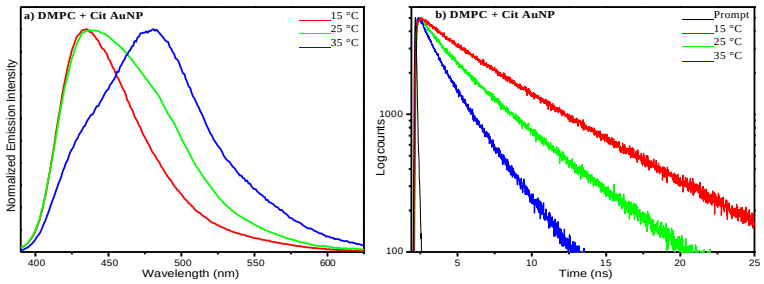

Figure 15: Changes in the steady state (a) and lifetime decay spectra (b) upon changing the temperature from 15 °C to 35 °C for DMPC-PRODAN system after addition of Cit-AuNPs. [PRODAN] = 2 µM, [DMPC] = 0.6 mM and [Cit-AuNPs] = 5.4 nM.

3.3) Probing the interaction of Au NPs with lipid bilayer using ANS: It is well known that ANS exhibits an emission spectra at 520 nm in the aqueous phase. However, in a less polar medium, i.e. lipid bilayers, it shows a remarkable blue shift in the emission spectra and a peak appears at 475-480 nm, followed by a huge increment (~80 times) in the fluorescence intensity. **Figure 16** reveals the fate of ANS-bound DMPC upon addition of various anionic AuNPs.

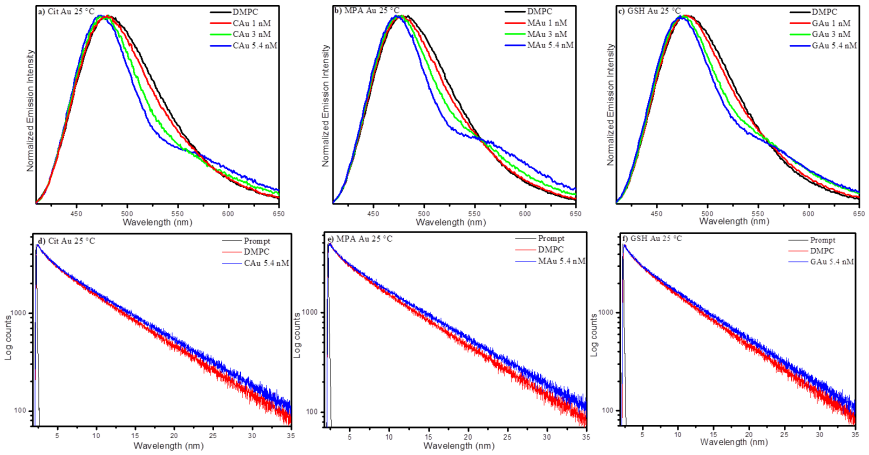

Figure 16: Normalized emission spectra for the addition of AuNPs in different concentrations (0 to 5.4 nM) to DMPC−ANS solution for (a) Citrate AuNPs, (b) MPA AuNPs, and (c) GSH AuNPs, and corresponding Time-resolved decay curves of ANS in DMPC−AuNPs solutions at 480 nm (d-f) at 25 °C.

TABLE 4 : @480 nm						
Sample	**τ_1 (ns)**	**τ_2 (ns)**	**a_1**	**a_2**	**χ^2**	**<T>(ns)**
DMPC	0.84	7.30	0.30	0.70	1.07	5.35
DMPC + Cit- AuNPs	1.35	8.83	0.27	0.73	1.04	6.81
DMPC + MPA-AuNPs	1.17	8.84	0.27	0.73	1.11	6.74
DMPC + GSH-AuNPs	1.34	8.82	0.26	0.74	1.01	6.85

Experimental error is within 5-10%

Table 4: Lifetime Components, Normalized Amplitudes of Lifetime Components, and Average Lifetime of ANS in the presence of DMPC, at Different Concentrations of Au NPs at 480 nm at 25 °C.

It is quite clear that the emission spectra of ANS present in the bilayer shows a blue shift upon interaction with Au NPs. It is a well-known fact that Au NPs moiety binds non-covalently to the lipid headgroup in the interfacial polar region and the hydrocarbon core of the phospholipid bilayer. The aniline group of ANS incorporates into the hydrocarbon layer whereas naphthalene and sulphonate group reside in the polar headgroup region. ANS lies near the hydrophilic interfacial region of the lipid bilayer being a charged species [55, 60-61]. The shifting of the emission spectra of ANS upon addition of AuNPs to the lipid bilayer indicates stabilization of the bilayer. Since the expeiment was performed at 25 °C, DMPC remains in nearly LC state, thus even a little change in the emission spectra can be easily detected.

Interestingly, we observe from **Figure 16 (a-c)** that in the emission spectra of ANS, a peak at around 520-530 nm starts to emerge after the addition of Au NPs. The reason behind this is that ANS, which is loosely bound to the bilayer surface and has a high sensitivity towards the membrane polarity,

starts to leak when Au NPs are added. Hence, the peak corresponding to the partitioning of ANS in aqueous medium appears at a higher wavelength.

For further insight, we conducted the liftime measurements of ANS in the presence of DMPC, upon addition various anionic AuNPs, and collected the decay at 480 nm as shown in **Figure 16 (d-e)**. It is evident from lifetime decay parameters **(Table 4)** that the lifetime at 480 nm increases upon addition of all the AuNPs. The decay parameters of ANS in DMPC are biexponential in nature. This indicates that ANS is heterogeneously distributed, although it resides mostly in the interfacial region of the bilayer. This is probably due to different modes of interaction of ANS with the lipid headgroups. Our results are in agreement with Misra *et al*[42] From the results in **Table 4**, it is observed that the longer components τ_2 increased from 7.30 (only DMPC) to 8.83 ns for Citrate-Au NPs, to 8.84 ns for MPA-Au NPs and to 8.82 ns for GSH-Au NPs. It is caused due to increase in stability and rigidity of the lipid bilayer upon addition of Au NPs which results in higher values of lifetime decay parameters.

Since ANS is loosely bound to the bilayer as compared to PRODAN, the shifting of the emission peak and increment in lifetime is a bit subdued and the results are not as pronounced as in the case of PRODAN. It is well known that PRODAN partitions to a very high extent in the LC phase than in the gel phase. The hydrophobic interactions of PRODAN in the presence of lipid bilayer further makes this probe particularly sensitive to the packing properties of the bilayer surface. The molecules of PRODAN may be squeezed out from the ordered and compact SG phase of the bilayer. This makes PRODAN more interesting to study any surface interactions. However, no such effect takes place in case of ANS.

3.4) Confocal imaging of the lipid bilayer and surface modification upon its interaction with Au NPs: The Confocal Laser Scanning Microscopy (CLSM) Imaging for the DMPC lipid bilayer, and that of the bilayer upon interaction with Au NPs was performed, as illustrated in **Figure 17**.

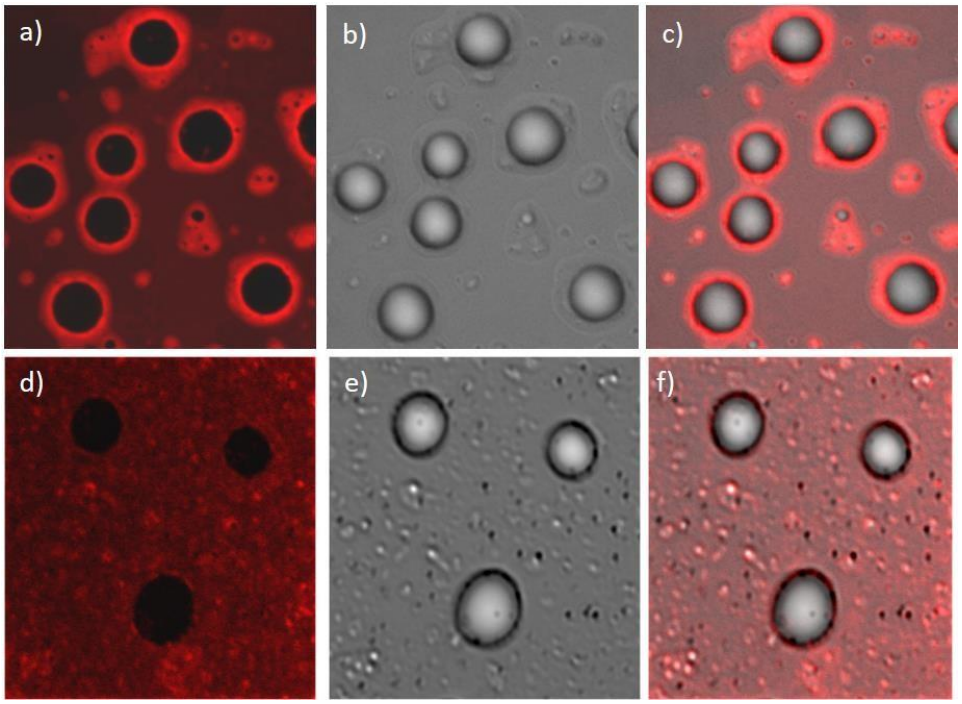

Figure 17: Au NP-DMPC bilayer interaction from Confocal Laser Scanning Microscopy (CLSM). Confocal, bright field and merged images for blank DMPC liposomes (a-c); and for DMPC-Au NP systems (d-f).

CHAPTER 4: CONCLUSION

It is concluded that anionic Au NPs interact quite strongly with the lipid bilayers making it more stable. The extent of interaction of these nanoparticles with the bilayer depends upon the bulkiness of the surface ligands used to functionalize these nanoparticles. From the steady-state and time resolved data it is confirmed that Citrate-Au NPs, having the least bulky surface ligands, interact the strongest with the lipid bilayer. In case of MPA- and GSH functionalized Au NP, the core of the Au NP becomes increasing distant from the lipid bilayer, due to increase in the bulkiness of the surface ligands. This results in weaker interaction of the nanoparticle with the bilayer. Moreover, the interaction of the lipid bilayer with the Au NPs is the strongest near the phase transition of the lipid molecule as compared to any other temperature in which the lipid bilayer is completely LC or SG phase. The confocal laser scanning microscopy (CLSM) imaging demonstrates the surface modification due to these interactions on the bilayer.

REFERENCES

[1] Wikipedia, https://en.wikipedia.org/wiki/Liposome.

[2] Tsukada, *et al* (2015), Spectroscopic and Morphological Studies on Interaction between Gold Nanoparticle and Liposome Constructed with Phosphatidylcholine, IOP CONF. SER. MATER. SCI, 76, 012001 (DOI: 10.1088/1757-899X/76/1/012001)

[3] Kanwa, *et al* (2017), Spectroscopic Study of the Interaction of Carboxyl-Modified Gold Nanoparticles with Liposomes of Different Chain Lengths and Controlled Drug Release by Layer-by-Layer Technology, J. Phys. Chem. B, 121, 11333–11343 (DOI: 10.1021/acs.jpcb.7b08455)

[4] Thamphiwatana, *et al* (2013), Nanoparticle-Stabilized Liposomes or pH-Responsive Gastric Drug Delivery, Langmuir, 29, 12228−12233 (DOI: 10.1021/la402695c)

[5] Adhikari, *et al* (2015), Controlled Release of a Sparingly Water-Soluble Anticancer Drug through pH-Responsive Functionalized Gold-Nanoparticle-Decorated Liposomes, ChemPhysChem, 16, 866−871 (DOI: 10.1002/cphc.201402748)

[6] Pornpattananangkul, *et al* (2010), Stimuli-Responsive Liposome Fusion Mediated by Gold Nanoparticles, ACS Nano, 4, 1935−1942 (DOI: 10.1021/nn9018587)

[7] Yu, *et al* (2007), Cationic Nanoparticles Stabilize Zwitterionic Liposomes Better than Anionic Ones, J. Phys. Chem. C, 111, 8233-8236 (DOI: 10.1021/jp072680z)

[8] De, *et al* (2018), Spectroscopic Evidence for Hydration and Dehydration of Lipid Bilayers upon Interaction with Metal Ions: A New Physical Insight, Phys. Chem. Chem. Phys., 20, 14796-14807 (DOI: 10.1039/C8CP01774C)

[9] Binder, *et al* (2002), The Effect of Metal Cations on the Phase Behavior and Hydration Characteristics of Phospholipid Membranes, Chemistry and physics of lipids, 115, 39–61 (DOI: 10.1016/s0009-3084(02)00005-1)

[10] Hong, Tamm, (2004), Elastic Coupling of Integral Membrane Protein Stability to Lipid Bilayer Forces. Proc. Natl. Acad. Sci. U.S.A., 101, 4065–4070 (DOI: 10.1073/pnas.0400358101)

[11] Vafaei, *et al* (2017), Optimizing the Performance of Supported Lipid Bilayers as Cell Culture Platforms Based on Extracellular Matrix Functionalization, ACS Omega, 2, 2395−2404 (DOI: 10.1021/acsomega.7b00158)

[12] Zumbuehl, Weder, (1981), Liposomes of Controllable Size in the Range of 40 to 180 nm by Defined Dialysis of Lipid/Detergent Mixed Micelles, Biochim. Biophys. Acta, Biomembr, 640, 252– 262 (DOI: 10.1016/0005-2736(81)90550-2)

[13] Szoka, Papahadjopoulos, (1978), Procedure for Preparation of Liposomes with Large Internal Aqueous Space and High Capture by Reverse-Phase Evaporation, Proc. Natl. Acad. Sci. U. S. A., 75, 4194– 4198

[14] Bangham, *et al* (1967), Osmotic Properties and Water Permeability of Phospholipid Liquid Crystals, Chem. Phys. Lipids, 1, 225– 246 (DOI: 10.1016/0009-3084(67)90030-8)

[15] Deamer, Bangham, (1976), Large Volume Liposomes by an Ether Vaporization Method. Biochim. Biophys. Acta, Biomembr,. 443, 629–634 (DOI: 10.1016/0005-2736(76)90483-1)

[16] Avanti Polar Lipids, Inc., https://avantilipids.com/tech-support/faqs/transition-temperature

[17] Sunamoto, *et al* (1980), Liposomal Membranes. VI. Polysaccharide-Induced Aggregation of Multilamellar Liposomes of Egg Lecithin, Journal of Biochemistry, 88, 1219

[18] Massenburg, Lentz, (1993), Poly(ethylene glycol)-Induced Fusion and Rupture of dipalmitoylphosphatidylcholine Large, Unilamellar Extruded Vesicles, Biochemistry, 32, 9172

[19] Viguera, *et al* (1993), Liposome Aggregation Induced by poly(ethylene glycol) : Rapid Kinetic Studies, Biochemistry, 32, 3708 (DOI: 10.1016/0927-7765(94)01138-U)

[20] Viguera, *et al* (1995), Aggregation of Phospholipid Vesicles by Water-Soluble Polymers. Colloids Surf., B, 3, 263(DOI: 10.1016/S0006-3495(96)79452-3)

[21] Lis, *et al* (1982), Interactions between Neutral Phospholipid Bilayer Membranes. Biophys. J., 37, 657.

[22] Sankaram, Thompson. (1991), Cholesterol-Induced Fluid-Phase Immiscibility in Membranes. Proc. Natl. Acad. Sci. U.S.A., 88, 8686-8690.

[23] de Almeida, *et al* (2003), Sphingomyelin / Phosphatidylcholine / Cholesterol Phase Diagram: Boundaries and Composition of Lipid Rafts. Biophys. J., 85, 2406–2416 (DOI: 10.1016/S0006-3495(03)74664-5)

[24] Raffy, JTeissi, (1999), Control of Lipid Membrane Stability by Cholesterol Content. Biophys. J., 76, 2072–2080 (DOI: 10.1016/S0006-3495(99)77363-7)

[25] Rog, *et al* (2009), Ordering Effects of Cholesterol and its Analogues. Biochim. Biophys. Acta, Biomembr., 1788, 97–121(DOI: 10.1016/j.bbamem.2008.08.022)

[26] Al-Jamal, Kostarelos. (2007), Liposome-Nanoparticle Hybrids for Multimodal Diagnostic and Therapeutic Applications. Nanomedicine, 2, 85-98(DOI: 10.2217/17435889.2.1.85)

[27] Preiss, Bothun. (2011), Stimuli-Responsive Liposome Nanoparticle Assemblies. Expert Opin. Drug Delivery, 8, 1025-1040.

[28] Paasonen, *et al* (2010), Gold-Embedded Photosensitive Liposomes for Drug Delivery: Triggering Mechanism and Intracellular Release. J. Control. Release, 147, 136-143(DOI: 10.1016/j.jconrel.2010.07.095)

[29] Liu, *et al* (2009), Electrostatically Mediated Liposome Fusion and Lipid Exchange with a Nanoparticle Supported Bilayer for Control of Surface Charge, Drug Containment, and Delivery. J. Am. Chem. Soc., 131, 7567-7569(DOI: 10.1021/ja902039y)

[30] Tan, *et al* (2013), Lipid-Enveloped Hybrid Nanoparticles for Drug Delivery. Nanoscale, 5, 860-872(DOI: 10.1039/c2nr32880a)

[31] Abraham, Narine. (2011), A Facile Synthesis of Lipid Stabilized Gold Nanoparticles: A Step Towards Biodegradable Biosensors. J. Nanosci. Nanotechnol., 11, 7027-32

[32] Huang, *et al* (2009), Formulation of Novel Lipid-Coated Magnetic Nanoparticles as the Probe for In Vivo Imaging. J. Biomed. Sci., 16, 86 (DOI: 10.1186/1423-0127-16-86)

[33] Castellana, *et al* (2011), Label-Free Biosensing with Lipid-Functionalized Gold Nanorods, J. Am. Chem. Soc., 133, 4182-4185 (DOI: 10.1021/ja109936h)

[34] Mansoori, *et al* (2012), A Review on Liposome, IJARPB, 2, 453-464.

[35] Akhbarzade, *et al* (2013), Liposome: Classification, Preparation, and Applications, Nanoscale Res Lett., 8, 102 (DOI : 10.1186/1556-276X-8-102)

[36] Seema, *et al* (2012), Liposomes: Preparations and Applications, Int. J. Drug Dev. & Res., 4, 108-115.

[37] Wang, *et al* (2008), Nanoparticle-Induced Surface Reconstruction of Phospholipid Membranes, Proc. Natl. Acad. Sci. U. S. A., 105, 18171-18175.(DOI: 10.1073/pnas.0807296105)

[38] Wang, Liu. (2015), A Stable Lipid/TiO_2 Interface with Headgroup Inversed Phosphocholine and a Comparison with SiO_2, J. Am. Chem. Soc., 137, 11736-11742(DOI: 10.1021/jacs.5b06642)

[39] Zhang, Granick. (2006), How to Stabilize Phospholipid Liposome (Using Nanoparticles), Nano Lett., 6, 694-698. (DOI: 10.1021/nl052455y)

[40] Ganeshan, *et al* (2007), Monodisperse Thioether-Stabilized Palladium Nanoparticles: Synthesis, Characterization, and Reactivity, Chem. Mater., 19, 3464–3471 (DOI: 10.1021/cm062655q)

[41] Mieszawska, *et al* (2013), Multifunctional Gold Nanoparticles for Diagosis and Therapy of Disease, Mol. Pharmaceutics, 10, 831–847(DOI: 10.1021/mp3005885)

[42] Mattoussi, *et al* (2012), Luminescent Quantum Dots as Platforms for Probing In Vitro and In Vivo Biological Processes, Adv. Drug Delivery Rev., 64, 138– 166 (DOI: 10.1016/j.addr.2011.09.011)

[43] Al-Jamal, Kostarelos. (2011), Liposomes: From a Clinically Established Drug Delivery System to a Nanoparticle Platform for Theranostic Nanomedicine, Acc. Chem. Res., 44, 1094– 1104 (DOI: 10.1021/ar200105p)

[44] Preiss, Bothun. (2011), Stimuli-Responsive Liposome- Nanoparticle Assemblies, Expert Opin. Drug Delivery, 8, 1025– 1040 (DOI: 10.1517/17425247.2011.584868)

[45] Reimhul, E. (2015), Nanoparticle-Triggered Release from Lipid Membrane, Vesicles New Biotechnol., 32, 665–672

[46] Brayner, *et al* (2010), ZnO Nanoparticles: Synthesis, Characterization, and Ecotoxicological Studies, Langmuir, 26, 6522–6528(DOI: 10.1021/la100293s)

[47] Das, *et al* (2016), Mn_5Si_3 Nanoparticles: Synthesis and Size-Induced Ferromagnetism, Nano Lett., 16, 1132– 1137(DOI: 10.1021/acs.nanolett.5b04360)

[48] Gao, *et al* (2012), Colloidal Stability of Gold Nanoparticles Modified with Thiol Compounds: Bioconjugation and Application in Cancer Cell Imaging, Langmuir, 28, 4464-4471(DOI: 10.1021/la204289k)

[49] Zhao, *et al* (2017), Colorimetric Detection of Streptomycin in Milk Based on Peroxidase-Mimicking Catalytic Activity of Gold Nanoparticles, RSCAdv.,7,38471-38478(DOI: 10.1039/C7RA06434A)

[50] Piella, *et al* (2016), Size-Controlled Synthesis of Sub- 10-nanometer Citrate-Stabilized Gold Nanoparticles and Related Optical Properties, Chem. Mater., 28, 1066-1075(DOI: 10.1021/acs.chemmater.5b04406)

[51] Maguraa, *et al* (2014), Thiol- Modified Gold Nanoparticles Deposited on Silica Support Using Dip Coating, Appl. Surf. Sci., 315, 392–399(DOI: 10.1016/j.apsusc.2014.07.173)

[52] Rance, *et al* (2010), van der Waals Interaction between Nanotubes and Nanoparticles for Controlled Assembly of Composite Nanostructures, ACS Nano, 4, 4920-4928(DOI: 10.1021/nn101287u)

[53] Mustafa, *et al* (2010), Surface Plasmon Coupling Effect of Gold Nanoparticles with Different Shape and Size on Conventional Surface Plasmon Resonance Signal, Plasmonics, 5, 221-231(DOI: 10.1007/s11468-010-9141-z)

[54] Wang, *et al* (2012), Near- and Far-Field Effects on the Plasmon Coupling in Gold Nanoparticle Arrays, J. Phys. Chem. C, 116, 24741-24747(DOI: 10.1021/jp306292r)

[55] Mohapatra, Mishra. (2013), Photophysical Behavior of 8-Anilino-1-Naphthalenesulfonate in Vesicles of Pulmonary Surfactant Dipalmitoylphosphatidylcholine (DPPC) and Its Sensitivity toward the Bile Salt−Vesicle Interaction, Langmuir, 29, 11396-11404.

[56] Parasassi, *et al* (1998), Laurdan and Prodan as Polarity-Sensitive Fluorescent Membrane Probes, J. Fluoresc., 8, 365−373(DOI: 10.1021/la402355j)

[57] Krasnowska, *et al* (1998), Prodan as a Membrane Surface Fluorescence Probe: Partitioning between Water and Phospholipid Phases, Biophy. J., 74, 1984-1993(DOI: 10.1016/S0006-3495(98)77905-6)

[58] Wilson-Ashworth, *et al* (2006), Differential Detection of Phospholipid Fluidity, Order, and Spacing by Fluorescence Spectroscopy of Bis-pyrene, Prodan, Nystatin, and Merocyanine. 540. Biophys. J., 91, 4091-4101(DOI: 10.1529/biophysj.106.090860)

[59] Novaira, *et al* (2007), New Insights on the Photophysical Behavior of PRODAN in Anionic and Cationic Reverse Micelles: From which State or States does it Emit? , J. Phys. Chem. B, 111, 748-759(DOI: 10.1021/jp065528q)

[60] Gutowicz, Krawczyk. (1986), Effect of 1-Anilinonaphthalene-8-Sulphonate on Phase Transition Temperature of Dipalmitoylphosphatidylcholine Liposomes, Chem. Phys. Lipids, 39, 357-364(DOI: 10.1016/0009-3084(86)90117-9)

[61] Lesslauer, *et al* (1972), X-ray Diffraction Studies of Lecithin Bimolecular Leaflets with Incorporated Fluorescent Probes, Proc. Natl. Acad. Sci. U.S.A., 69, 1499-1503.

[62] Lesslauer, *et al* (1971), On the Location of 1-Anilino-8- Naphthalene-Sulfonate in Lipid Model Systems: an X-Ray Diffraction Study, Biochim. Biophys. Acta, Biomembr., 241, 547-566(DOI: 10.1016/0005-2736(71)90054-X)

[63] Gulik-Krzywicki, *et al* (1970), Correlations between Structure and Spectroscopic Properties in Membrane Model Systems Trytophan and I-Anilino-8-Naphtalene Sulfonate Fluorescence in Protein-Lipid-Water Phases, Biochim. Biophys. Acta, Biomembr., 219, 1-10.

[64] Kosower, Kanety. (1983), Intramolecular Donor-Acceptor Systems. 10. Multiple Fluorescences from 8-(Phenylamino) 1-Naphthalenesulfonates, J. Am. Chem. Soc., 105, 6236-6243(DOI: 10.1021/ja00358a008)

[65] Wang, Liu. (2015), Self-Healable and Reversible Liposome Leakage by Citrate-Capped Gold Nanoparticles: Probing the Initial Adsorption/Desorption Induced Lipid Phase Transition, Nanoscale,, 7, 15599-15604(DOI: 10.1039/c5nr04805b)

[66] Bastus, *et al* (2011), Kinetically Controlled Seeded Growth Synthesis of Citrate-Stabilized Gold Nanoparticles of up to 200 nm: Size Focusing versus Ostwald Ripening, Langmuir, 27, 11098-11105(DOI: 10.1021/la201938u)

[67] Sen, Patra. (2009), Formation of Self-Assembled Au Nanoparticles and the Study of Their Optical Properties by Steady-State and Time-Resolved Spectroscopies, J. Phys. Chem. C, 113, 13125-13132 (DOI: 10.1021/jp9024188)

[68] Montis, *et al* (2014), Interaction of Nanoparticles with Lipid Membranes, a Multiscale Perspective, Nanoscale, 6, 6452-6457(DOI: 10.1039/C4NR00838C)

[69] Bhat, *et al* (2016), Effects of Gold Nanoparticles on Lipid Packing and Membrane Pore Formation, Appl. Phys. Lett., 109, 263106 (1-5)(DOI: 10.1063/1.4972868)

[70] Garcia-Manyes, *et al* (2005), Effect of Temperature on the Nanomechanics of Lipid Bilayers Studied by Force Spectroscopy, Biophys. J., 89, 4261-4271(DOI: 10.1529/biophysj.105.065581)

[71] Urban, *et al* (2016), Reversible Control of Current across Lipid Membranes by Local Heating, Sci. Rep., 6, 22686(DOI: 10.1038/srep22686)

[72] Morinia, *et al* (2015), Influence of Temperature, Anions and Size Distribution on the Zetapotential of DMPC, DPPC and DMPE lipid vesicles, Colloids Surf. B, 131, 54-58(DOI: 10.1016/j.colsurfb.2015.03.054)

* http://www.fluorophores.tugraz.at/substance/603

**https://www.sigmaaldrich.com/catalog/product/sigma/41525?lang=en&region=IN